Comparison of CMIP5 and CMIP6 GCM performance for flood projections in the Mekong River Basin

AUTHOR(S):

Try, Sophal; Tanaka, Shigenobu; Tanaka, Kenji; Sayama, Takahiro; Khujanazarov, Temur; Oeurng, Chantha

CITATION:

Try, Sophal ...[et al]. Comparison of CMIP5 and CMIP6 GCM performance for flood projections in the Mekong River Basin. Journal of Hydrology: Regional Studies 2022, 40: 101035.

ISSUE DATE:

2022-04

URL:

http://hdl.handle.net/2433/275985

Journal of Hydrology: Regional Studies 40 (2022) 101035

Contents lists available at ScienceDirect

Journal of Hydrology: Regional Studies

journal homepage: www.elsevier.com/locate/ejrh

Comparison of CMIP5 and CMIP6 GCM performance for flood projections in the Mekong River Basin

Sophal Try [a,b,*], Shigenobu Tanaka [a], Kenji Tanaka [a], Takahiro Sayama [a], Temur Khujanazarov [a], Chantha Oeurng [b]

[a] Disaster Prevention Research Institute, Kyoto University, Gokasho, Uji 611-0011, Japan
[b] Faculty of Hydrology and Water Resource Engineering, Institute of Technology of Cambodia, Russian Conf. Blvd., Phnom Penh 12156, Cambodia

ARTICLE INFO

Keywords:
CMIP5
CMIP6
GCM
Flooding
Mekong River Basin

ABSTRACT

Study region: Mekong River Basin.
Study focus: The Coupled Model Intercomparison Project Phase 6 (CMIP6) recently announced an updated version of general circulation models (GCMs). This study investigated the performance of improved CMIP6 over those of CMIP5 with respect to precipitation and flood representations in the Mekong River Basin (MRB). The correlation and error comparison from the referenced precipitation exhibited a significant improvement in the peak value representation. Hence, the impacts of climate change on future floods in the MRB were simulated and assessed using a distributed rainfall–runoff–inundation model.
New hydrological insights for the region: The results indicated that precipitation from CMIP6 had a higher correlation and a lower error coefficient than CMIP5. Similarly, the simulation of GCM ensembles of monthly discharge from CMIP6 exhibited a comparable average value to the observations, whereas CMIP5 underestimated the discharge simulations. The performance of the mean annual peak discharge improved from 37,220 m^3/s (CMIP5) to 45,423 m^3/s (CMIP6) compared to 43,521 m^3/s (observation). The projections of future floods in the MRB from CMIP6 exhibited an increase of annual peak discharge at Chiang Saen, Vientiane, Pakse, and Kratie stations by 10–15%, 20–22%, and 24–29% for the SSP2-4.5 scenario, and 10–18%, 24–29%, and 41–54% for the SSP5-8.5 scenario in the near future (2026–2050), mid-future (2051–2075), and far future (2076–2100), respectively. The statistical K-S test showed significant changes in all stations and projected periods with a p-value < 0.01.

1. Introduction

With a drainage area of 795,000 km^2, the Mekong River Basin (MRB) is one of the largest transboundary rivers shared by China, Myanmar, Thailand, Lao People's Democratic Republic (Lao PDR), Cambodia, and Vietnam. The floodplain and delta areas located in the Lower Mekong Basin (LMB) are annually affected by flooding as a natural phenomenon leading to the deposition of sediment as a natural fertilizer, resulting in high agricultural productivity and biodiversity. However, the frequency and severity of extreme flood events over the last few decades and future projections would be significantly increased (Hoang et al., 2016; Oddo et al., 2018; Perera et al., 2017; Try et al., 2020a; Västilä et al., 2010). Flood-related economic damage has also risen (Try et al., 2018a), primarily because

* Corresponding author at: Disaster Prevention Research Institute, Kyoto University, Gokasho, Uji 611-0011, Japan.
E-mail address: try.sophal.a92@kyoto-u.jp (S. Try).

https://doi.org/10.1016/j.ejrh.2022.101035
Received 1 November 2021; Received in revised form 8 February 2022; Accepted 9 February 2022
Available online 11 February 2022

of the significant increase in population and settlement close to the river network and floodplain of the LMB (Try et al., 2018a). The cost of the average historical annual flood damage is approximately US$ 60–70 million, and these figures continue to rise (MRC, 2011).

Climate change and human activity are projected to affect the hydrological and ecological systems of the LMB, particularly in Tonle Sap Lake (Chadwick and Juntopas, 2008; Hoang et al., 2016; Johnstone et al., 2013; Keskinen et al., 2013; Try et al., 2020a, 2020b; Uk et al., 2018). The Tonle Sap Lake and its floodplain play a significant role in the hydrology of the LMB. The Tonle Sap River (the connection between the Mekong River and Tonle Sap Lake) has a bi-directional flow between the rainy and dry seasons. This area is home to more than 370 plant species, 197 phytoplankton species, and more than 225 bird species (MRC, 2010). Constant assessment of the projected impacts of future climate on regional infrastructure and the environment is essential to be able to develop and implement appropriate adaptation measures.

Flood simulations in the Mekong region have been studied extensively. For instance, Try et al. (2018b) simulated a large-scale flood inundation in the entire MRB during the large flood event in 2000. Wang et al. (2021b) simulated daily floods in the MRB from 1967 to 2015. Pokhrel et al. (2018) studied flood dynamics in the LMB, focusing on the variations in upstream flow regulation. Siev et al. (2019) and Tanaka et al. (2018) modeled the inundation pattern in Tonle Sap Lake, a major sub-basin in the LMB.

Future planning, preparation, mitigation, and adaptation measures in river basins are essential in the current reality of climate change. Thus, information on climate change effects on a river basin is vital to policymakers and the population in general. General circulation model (GCM) uncertainties have been identified from different sources, such as the assumption of greenhouse gas emission scenarios, model configuration, climate downscaling, and the unforced variability of the climate system (Giorgi, 2010), yet they still provide a valuable source of stochastic system performance. The Coupled Model Intercomparison Project Phase 5 (CMIP5) results have reduced the uncertainty of hydrological extremes under climate change in the MRB compared to CMIP3 (Hoang et al., 2016).

The Intergovernmental Panel on Climate Change (IPCC) recently released new outputs from CMIP6. The CMIP5 projected the future climate based on greenhouse gas emissions represented by four representative concentration pathways (RCPs), namely RCP2.6, RCP4.5, RCP6.0, and RCP8.5 (IPCC, 2014). The CMIP6 has designed five scenarios called shared socioeconomic pathways (SSP), namely SSP1-2.6, SSP2-4.5, SSP4-6.0, and SSP5-8.5, to include socioeconomic factors such as the growth of population, economics, urbanization and other factors (Eyring et al., 2016; O'Neill et al., 2016). The improvement of CMIP6 scenarios includes wider equilibrium climate sensitivity (ECS) with an increasing temperature range of 1.5–4.5 °C. The models in CMIP6 were expected to improve their capability and reduce uncertainty over the previous CMIP5 and CMIP3 (Chen et al., 2020). The new protocol of CMIP6 provided also the high-resolution GCM simulations (namely HighResMIP experiments) together with their coarse-resolution GCM, (Haarsma et al., 2016). The HighResMIP experiments would solve the issue of coarse resolution of climate models, with their resolutions being comparable to regional climate models (RCMs) (e.g., CORDEX) and high-resolution AGCM (Mizuta et al., 2012, 2014) in CMIP5.

Ruan et al. (2018) evaluated the ranking scores of precipitation from CMIP5 over the LMB. Chhin and Yoden (2018) proposed a framework for model ensemble selection based on historical simulations of CMIP5 in the Indochina region, and Chhin et al. (2020) used their optimal ensemble subset for future drought projections. Several studies on flood inundation simulation used a two-dimensional distributed model in the LMB during historical flood events (Dutta et al., 2007; Perera et al., 2017; Try et al., 2018b). Try et al. (2020b) assessed future climate change impacts on flood inundation in the LMB through a high-resolution atmospheric general circulation model from the Meteorological Research Institute (MRI-AGCM), in which sea surface temperatures (SSTs) from 28 CMIP5 were used as boundary condition. Try et al. (2020a) projected the extreme flood inundation in the MRB from a large ensemble database for policy decision making for future climate change (d4PDF) using MRI-AGCM with SST boundary conditions for six CMIP5 models: CCSM4, GFDL-CM3, HadGEM2, MIROC5, MPI-ESM-MR, and CGCM3. Overall, previous studies of future flooding projections in the MRB were based on previous CMIP3 and CMIP5 only.

A comparison of CMIP5 and CMIP6 could provide guidance for further exploration of the newly released CMIP6 datasets. CMIP6 are found to have an improved performance in capturing climate changes in various regions (Kamruzzaman et al., 2021; Wang et al., 2021a; Zamani et al., 2020). There is still a lack of information for the comparison of CMIP5 and CMIP6 on precipitation and flood projections in the Mekong region. Considering the significant improvement in the climate variables of the CMIP6 over CMIP5, it is necessary to conduct a comparative study that will provide a valuable resource of information for policy decision-makers in this area.

Iqbal et al. (2021) evaluated CMIP6 precipitation over mainland Southeast Asia, and results indicated that most CMIP6 models were able to capture rainfall climatological in this region. Gusain et al. (2020) found the improvements of precipitation in agreement with the observation from CMIP6 over CMIP5 in simulating the Indian summer monsoon. Moreover, Kim et al. (2020) analyzed extreme climate indices from CMIP6 models and showed their improved ability to capture the global and regional climate patterns. Demory et al. (2020) showed that RCM (EURO-CORDEX) and HighResMIP outperform CMIP5, particularly in summer and autumn in most of the European regions. Dong and Dong (2021) found an improvement in bias reduction of extreme precipitation in Asia from CMIP6 (coarse resolution and HighResMIP experiments) over CMIP5. Xin et al. (2021) revealed better performance of model ensemble from CMIP6 HighResMIP in simulation of precipitation distribution in China. The high resolution HighResMIP was found suitable for projecting of monsoon precipitation and hydrological extreme in case studies in Peninsular Malaysia (Liang et al., 2021; Tan et al., 2021).

This study aims to investigate the performance of CMIP6 compared to CMIP5 on precipitation estimates applied to flood simulation within the MRB. It also assesses the potential impacts of climate change on flood inundation in the MRB under the new projected scenarios for the near future (2026–2050), mid-future (2050–2075), and far future (2075 until the end of the 21st century).

2. Methodology

2.1. Rainfall–runoff–inundation modeling

This study used an integrated rainfall–runoff and flood inundation (RRI) model (Sayama et al., 2012, 2015a, 2015b). The RRI model is a two-dimensional distributed model that separately considers hill slopes and river channels. The RRI model calculates flow on slopes and rivers based on 2D and 1D diffusive wave equations, which can consider reversed flow. The RRI model simulates the lateral subsurface flow, vertical infiltration, and surface flow to represent the rainfall–runoff–inundation processes. The river geometry is assumed to be rectangular with width W [m] and depth D [m] as indicated in Eqs. (1) and (2) as a function of upstream drainage area A [km^2]. Try et al. (2018b) calculated the geometry coefficients C_W, S_W, C_D, and S_D with values of 0.0015, 0.7491, 0.0520, and 0.7596, respectively, for the MRB.

$$W = C_W A^{S_W} \tag{1}$$

$$D = C_D A^{S_D} \tag{2}$$

This study employed the precipitation dataset from GPCC with daily scale and 1° resolution (Ziese et al., 2018). The GPCC precipitation data provide a reasonable rainfall distribution over the entire MRB in the rainfall–runoff–inundation modeling by exhibiting a better correlation with the observed discharge than other available open datasets (Try et al., 2020c). Try et al. (2020a, 2020b) validated the GPCC data for long-term flood inundation modeling in the MRB for 1983–2010 and 1982–2007, respectively.

The evapotranspiration dataset was taken from the Japanese 55-year Reanalysis dataset (JRA-55) with 3-hourly and 0.5625° resolution (Kobayashi et al., 2015). The topography datasets, including digital elevation model (DEM), flow direction (DIR), and flow accumulation (ACC), derived from Multi-Error-Removed-Improved-Terrain (MERIT DEM, Yamazaki et al., 2017) and land use from MODIS (product: MCD12Q1) for 2000 (Friedl et al., 2010) were used as input to the RRI model in this study. More detailed description of model structure and input parameters of the RRI model could be found in the supplementary file.

The RRI model has been applied to hydrological simulations in Southeast Asia to simulate flood inundation and confirm its good performance. For example, the RRI model was used to reproduce a historical large-scale flood event in 2000 (Try et al., 2018b) and to evaluate the performance of satellite-based precipitation products for flood inundation simulation (Try et al., 2020c). Perera et al. (2017) and Try et al. (2020b) used the RRI model to evaluate the effects of climate change in the LMB by considering various RCP and SST scenarios. Moreover, Try et al. (2020a) validated the RRI model for long-term simulation (1983–2010) before using it to project extreme flood inundation events in the MRB.

Table 1
Description of climate datasets from CMIP5, CMIP6, HighResMIP, and CORDEX used in this study.

No.	Model Name		Resolution	Modeling Agency	References
	CMIP5	CMIP6	Lon. × Lat.		
1	CNRM-CM5	CNRM-CM6-1	1.40625 × 1.40625	Centre National de Recherches Meteorologiques, France	Voldoire et al. (2013)
	CNRM-CM6-1-HR[a]		0.5 × 0.5		
	CNRM-CERFACS-CNRM-CM5[b]		0.5 × 0.5		
2	IPSL-CM5A-LR	IPSL-CM6A-LR	2.5 × 1.25874	Institut Pierre-Simon Laplace, France	Dufresne et al. (2013)
3	MIROC5	MIROC6	1.40625 × 1.40625	Atmosphere and Ocean Research Institute, National Institute for Environmental Studies, Japan Agency for Marine-Earth Science and Technology, Japan	Watanabe et al. (2011)
4	MPI-ESM-LR	MPI-ESM1-2-LR	1.875 × 1.875	Max Planck Institute for Meteorology, Germany	Giorgetta et al. (2013)
	MPI-M-MPI-ESM-LR[b]		0.5 × 0.5		
5	MRI-ESM1	MRI-ESM2.0	1.125 × 1.125	Meteorological Research Institute, Japan	Yukimoto et al. (2012)
	MRI-AGCM3.2S[a]		0.1875 × 0.1875		
6	ACCESS1-3	ACCESS-CM2	1.875 × 1.25	Commonwealth Scientific and Industrial Research Organization and Bureau of Meteorology, Australia	Bi et al. (2013)
7	GFDL-CM3	GFDL-CM4	1.25 × 1.0[c]	Geophysical Fluid Dynamics Laboratory, USA	Donner et al. (2011)
8	NorESM1-M	NorESM2	1.25 × 0.9375[c]	Norwegian Climate Centre, Norway	Bentsen et al. (2013)

[a] High resolution GCMs from CMIP6 (HighResMIP experiments).
[b] Regional climate models from CORDEX East Asia (CORDEX-EA).
[c] The values describe the spatial resolution of CMIP6 while CMIP5 have double coarser resolution than CMIP6 in both longitude and latitude.

2.2. Climate datasets

Precipitation and evapotranspiration datasets were obtained from CMIP6 and CMIP5 at a daily time step. Eight GCMs were used for the comparative analysis. Each GCM was selected from the same institution in CMIP5 and CMIP6. Table 1 shows the institution, model name, and spatial resolution of each model. Six GCMs (No. 1 to No. 6 in Table 1) had the same spatial resolution in CMIP5 and CMIP6; two GCMs (Nos. 7 and 8) had a higher gridded resolution in CMIP6 than in CMIP5. To consider the effect of simulation of high resolution, this study compared two CMIP6 (CNRM-CM6-1 and MRI-ESM2.0) with two GCMs from HighResMIP (CNRM-CM6-1-HR and MRI-AGCM3.2S) and two RCMs from CORDEX East Asia (CNRM-CERFACS-CNRM-CM5 and MPI-M-MPI-ESM-LR). The GPCC rainfall dataset was used to evaluate the performance of GCMs from CMIP5 and CMIP6.

2.3. Performance assessment

This study used multiple statistical indicators to verify the performance of RRI model simulation, including Nash–Sutcliffe efficiency (NSE) (Nash and Sutcliffe, 1970), peak discharge ratio (PDR), and Kling–Gupta efficiency (KGE) (Gupta et al., 2009) which consists of three terms including β, α, and r:

$$\mathrm{NSE} = 1 - \frac{\sum_{t=1}^{n} (Q_s^t - Q_o^t)^2}{\sum_{t=1}^{n} (Q_o^t - \overline{Q_o})^2} \tag{3}$$

$$\mathrm{PDR} = \frac{Q_s^p}{Q_o^p} \tag{4}$$

$$\beta = \frac{\overline{Q_s}}{\overline{Q_o}} \tag{5}$$

$$\alpha = \frac{\sqrt{\frac{1}{n}\sum_{t=1}^{n} (Q_s^t - \overline{Q_s})^2}}{\sqrt{\frac{1}{n}\sum_{t=1}^{n} (Q_o^t - \overline{Q_o})^2}} \tag{6}$$

$$r = \frac{\sum_{t=1}^{n} (Q_s^t - \overline{Q_s})(Q_o^t - \overline{Q_o})}{\sqrt{\left(\sum_{t=1}^{n} (Q_o^t - \overline{Q_o})^2\right)\left(\sum_{t=1}^{n} (Q_s^t - \overline{Q_s})^2\right)}} \tag{7}$$

$$\mathrm{KGE} = 1 - \sqrt{(r-1)^2 + (\beta-1)^2 + (\alpha-1)^2} \tag{8}$$

where Q_s^t and Q_o^t are simulated and observed discharge at time step t, respectively; $\overline{Q_s}$ and $\overline{Q_o}$ are the mean simulated and observed discharge in the flood event, respectively; β and α are the measures of bias and variability, respectively; r is the correlation coefficient between simulation and observation; and Q_s^p and Q_o^p are simulated and observed peak discharge, respectively.

This study uses a Taylor diagram (Taylor, 2001) to quantify the pattern similarity between two variables (i.e., monthly precipitation from observations and GCMs). The standard deviations of the prediction (σ_p) and observation (σ_o), the correlation coefficient (r), and the statistical indicator of root mean square difference ($RMSD$) to quantify the difference between the two discrete variables p and o are determined as follows:

$$\sigma_f = \sqrt{\frac{1}{N}\sum_{n=1}^{N} (p_n - \overline{p})^2} \tag{9}$$

$$\sigma_o = \sqrt{\frac{1}{N}\sum_{n=1}^{N} (o_n - \overline{o})^2} \tag{10}$$

$$RMSD = \sqrt{\frac{1}{N}\sum_{n=1}^{N} [(p_n - \overline{p})(o_n - \overline{o})]^2} \tag{11}$$

where $\overline{p}$ and $\overline{o}$ are the mean values, N is the number of datasets that are both temporal and spatial patterns in this study.

The Taylor diagram provides a concise statistical summary of how well the pattern distribution of the two variables matches. The

diagram visualizes their correlation, root mean square difference, and variances of data (i.e., standard deviation). In this study, the Taylor diagram was used to visualize and evaluate the precipitation performance of CMIP5 and CMIP6 over the MRB. Geographical conditions and uneven precipitation distribution were estimated by dividing the MRB into three zones, namely, the Upper Mekong Basin in China, the middle MRB in Thailand and Lao PDR, and the LMB in Cambodia and Vietnam (Fig. 1). The simulated discharge from the RRI model from CMIP5 and CMIP6 in monthly and annual peak discharge values was compared with gauged observations. Finally, the best GCMs were selected for future projections to identify changes in flood characteristics in the MRB in the near, mid, and far future. The GCMs were bias-corrected for future flood projections. This study applied a bias correction method using linear scaling approach:

$$P_{day}^{BC} = \frac{P_{mon}^{obs}}{P_{mon}^{gcm}} \times P_{day}^{gcm} \tag{12}$$

where P_{mon}^{obs}: average monthly GPCC precipitation, P_{mon}^{gcm}: average monthly GCM precipitation, P_{day}^{agcm}: daily GCM precipitation, and P_{day}^{BC}: daily bias-corrected GCM precipitation. The correction factor calculated from the present climate was applied to future climate projections.

This study used the Kolmogorov–Smirnov (K–S) test to evaluate the changes in flooding between present and future projection climates. The statistical K–S test is a non-parametric test of two samples and is used to evaluate statistical variation. The maximum difference in the cumulative distribution function (CDF) of the two samples can be defined as follows:

$$D_{n,m} = \sup_x |F_n(x) - F_m(x)| \tag{13}$$

where F_n and F_m are the empirical distribution functions of the two samples, and sup is the supremum function. The null hypothesis, H_0, assumes that the two samples have no significant difference in the CDF. When the likelihood of the different distributions of the two

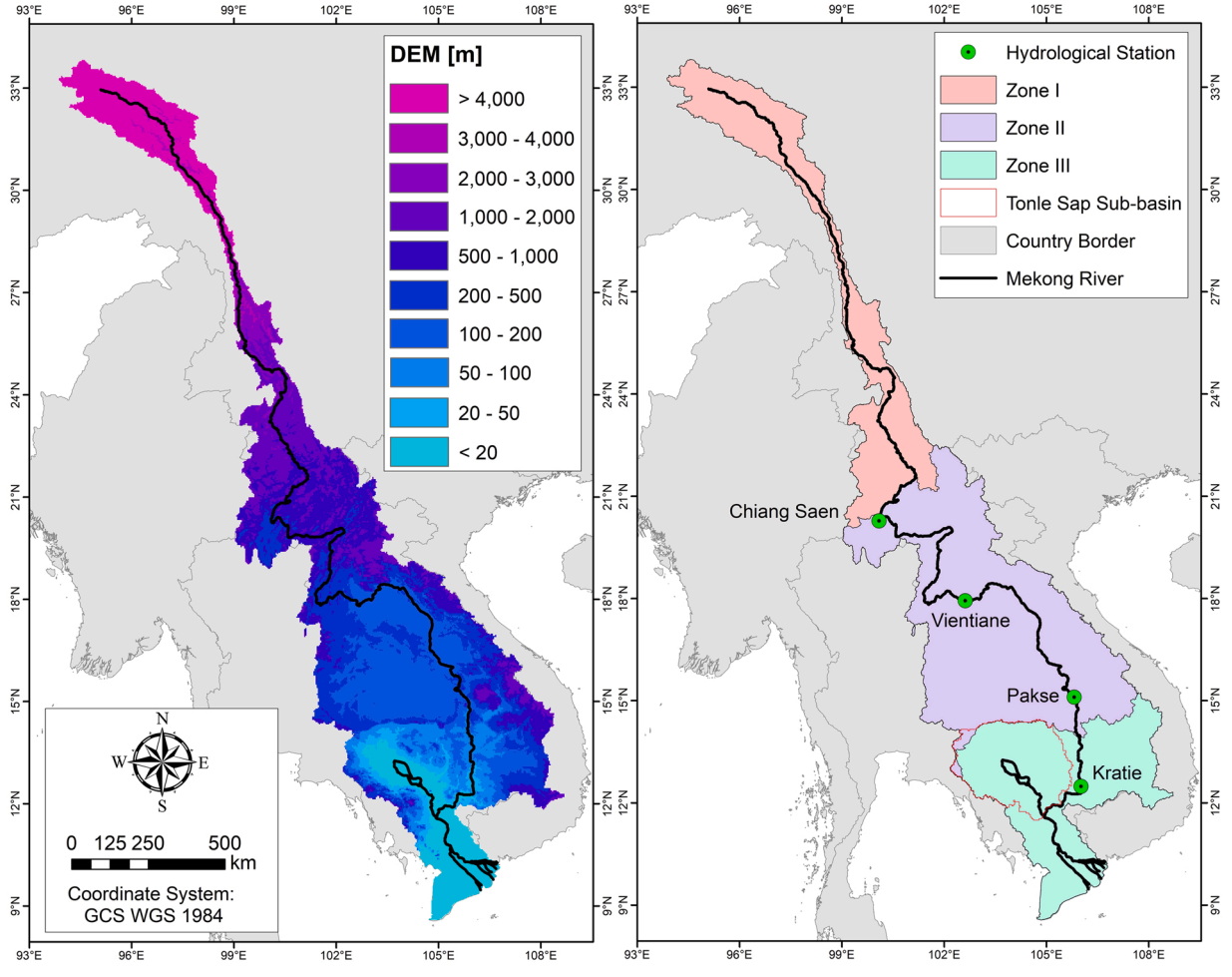

Fig. 1. Study area of the Mekong River Basin: a) digital elevation model (DEM) and b) three zones for precipitation evaluation.

samples exceeds the significance level, the null hypothesis is rejected. The null hypothesis is rejected if the following condition is satisfied:

$$D_{n,m} > c(\alpha)\sqrt{\frac{n+m}{nm}} \tag{14}$$

where n and m are the sample sizes. At a significance level of 1%, $c(\alpha)$ was equal to 1.628.

3. Results and discussion

3.1. RRI model performance

Fig. 2 compares the simulated discharge from the RRI model and the observed discharge at the four hydrological stations from upstream to downstream of the Mekong River at Chiang Saen, Vientiane, Pakse, and Kratie. The RRI model performance at the upstream station in Chiang Saen was KGE = 0.57, NSE = 0.49, r = 0.82, and PDR = 0.65 ± 0.15. The performance at the two middle stations of Vientiane and Pakse were KGE = 0.79 and 0.91, NSE = 0.74 and 0.85, r = 0.88 and 0.93, and PDR = 0.80 ± 0.14 and 0.95 ± 0.17, respectively. The RRI model simulated discharge was more accurate at the downstream station Kratie with KGE = 0.93, NSE = 0.88, r = 0.94, and PDR = 0.95 ± 0.15. Overall, the RRI model performance in the MRB hydrological simulation was acceptable and particularly accurate in the downstream area, which is the area most affected by floods.

3.2. Evaluation of precipitation

The historical GCM experiments used were from 1950 to 2005 for CMIP5 and from 1950 to 2014 for CMIP6. The monthly precipitation results based on the grid by grid distribution and basin average for each GCM from CMIP5 and CMIP6 are shown in the Taylor diagrams in Figs. 3 and 4, respectively. The basin average precipitation had higher accuracy than the grid by grid precipitation in the correlation coefficient (r), root mean square difference (*RMSD*), and standard deviation (σ). For the grid by grid precipitation, the improvement of GCMs was r = 0.48 and *RMSD* = 79.11 mm in CMIP5 to r = 0.58 and *RMSD* = 72.82 mm in CMIP6 (Table 2). The standard deviation values were similarly improved from σ = 61.81 mm in CMIP5 to σ = 67.10 mm in CMIP6 (σ of GPCC = 87.89 mm) (Table 2). For the basin average precipitation, the performance improvement from CMIP5 to CMIP6 was 0.97–0.99 for the correlation

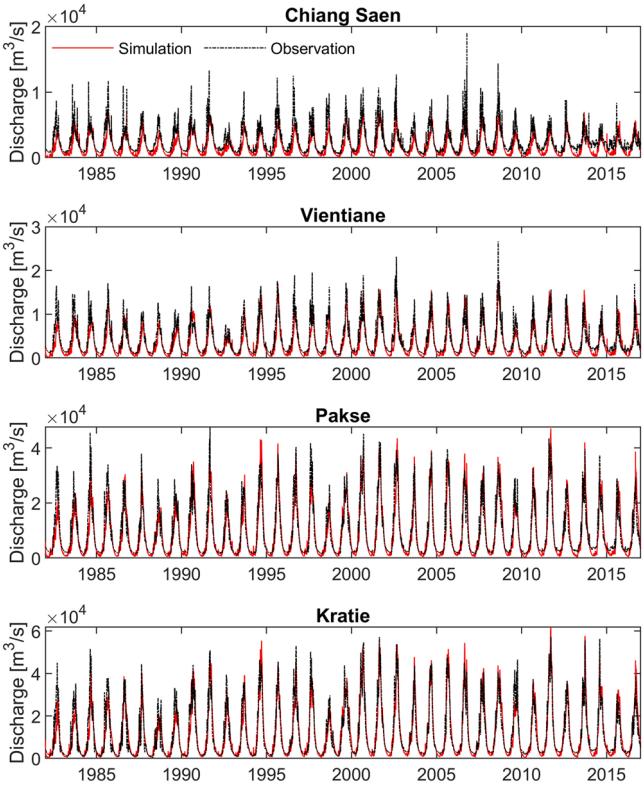

Fig. 2. Comparison of daily simulated and observed discharge at four stations (Chiang Saen, Vientiane, Pakse, and Kratie) along the main stream of the Mekong River between 1982 and 2016.

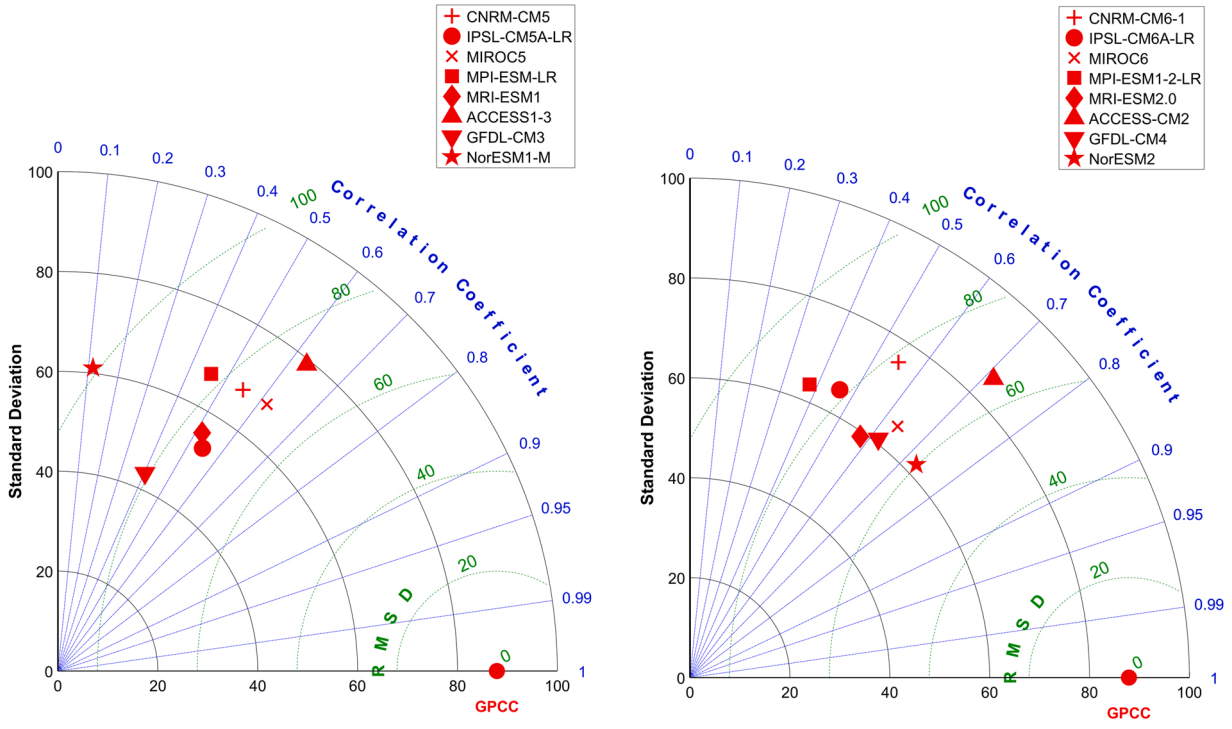

Fig. 3. Taylor diagram of average monthly precipitation for the grid by grid distribution from CMIP5 (left) and CMIP6 (right).

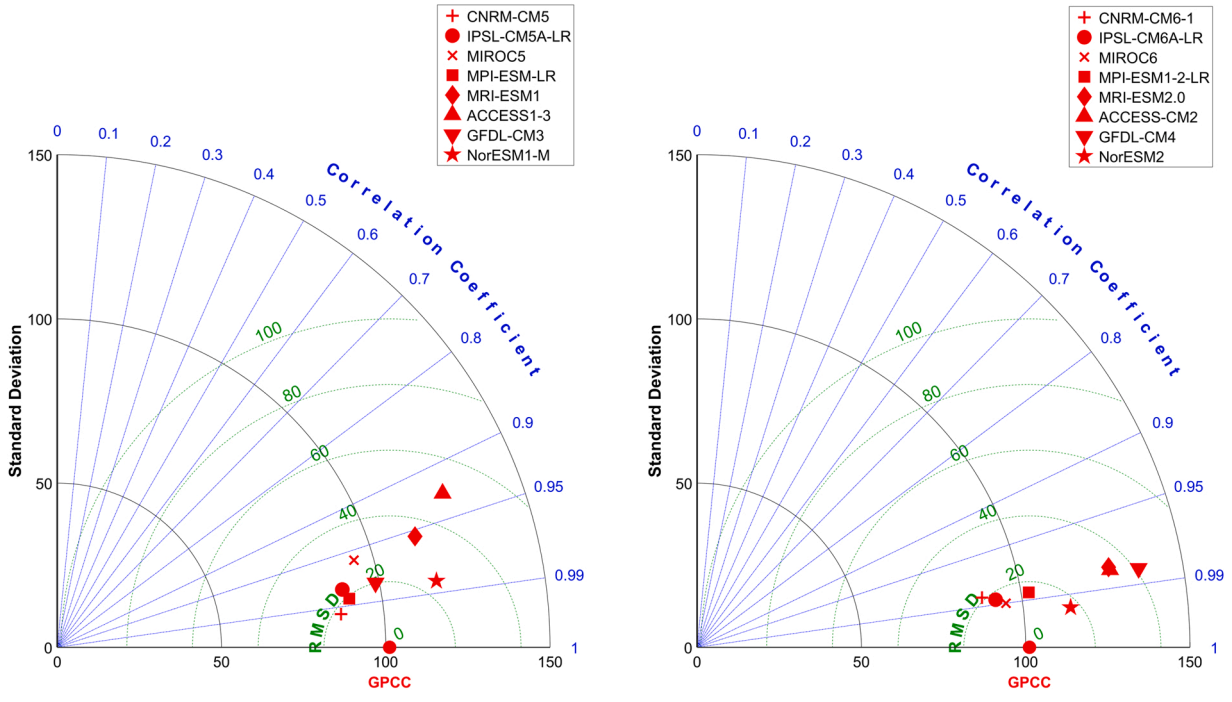

Fig. 4. Taylor diagram of average monthly precipitation for basin average for CMIP5 (left) and CMIP6 (right).

coefficient and 27.20–24.67 mm for the bias. However, the standard deviation seemed larger in CMIP6, being 110.46 mm compared to 102 mm in CMIP5 (σ of GPCC = 101.18 mm). This means that CMIP6 have improved their agreement with reference precipitation and have shown smaller error values in both analyses of the basin average and the grid by grid precipitation.

In addition to the evaluation based on the grid by grid and the basin average, the precipitation results were also compared for the

Table 2
Comparison of correlation coefficient (r), root mean square difference ($RMSD$), and standard deviation (σ) between grid by grid and basin average precipitation from CMIP5 and CMIP6.

GCMs		r [-]	$RMSD$ [mm]	σ [mm]		r [-]	$RMSD$ [mm]	σ [mm]
Grid by Grid	GPCC	–	–	87.89		–	–	87.89
	CMIP5	0.55	75.87	67.41	CMIP6	0.55	78.21	75.69
		0.54	73.93	53.18		0.46	81.69	64.95
		0.62	70.53	67.84		0.64	68.34	65.24
		0.46	82.52	66.92		0.38	86.78	63.39
		0.52	75.84	55.73		0.58	72.28	59.12
		0.63	72.21	79.04		0.71	65.67	85.26
		0.40	80.84	43.28		0.62	69.30	60.87
		0.11	101.11	61.08		0.73	60.27	62.24
	avg.	0.48	79.11	61.81		0.58	72.82	67.10
Basin Average	GPCC	–	–	101.18		–	–	101.18
	CMIP5	0.99	17.94	86.95	CMIP6	0.99	20.94	88.01
		0.98	22.74	88.54		0.99	17.79	92.00
		0.96	28.66	94.09		0.99	15.17	94.98
		0.99	19.26	90.10		0.99	16.73	102.33
		0.96	34.67	114.04		0.98	34.26	127.57
		0.93	49.55	126.30		0.98	34.02	127.89
		0.98	20.06	98.84		0.98	41.00	136.52
		0.99	24.74	117.18		0.99	17.46	114.35
	avg.	0.97	27.20	102.00		0.99	24.67	110.46

three zones: upstream high elevation, midstream, and downstream in the MRB. Both CMIP5 and CMIP6 generally exhibited good performance in Zone III (the LMB–floodplain and delta), followed by Zone II (central MRB) and Zone I (the Upper Mekong Basin), ranked by the best performance. The tendency of each model distribution in the Taylor plot in Fig. 5 can be distinguished by an increase in the correlation coefficient and a reduction in the bias index $RMSD$ from CMIP5 to CMIP6, particularly noticeable in Zones I and II. However, CMIP6 also had larger standard deviation values compared to CMIP5. Table 3 provides a summary of the information on all model performances. For Zone III, the average performance indices among eight GCMs were $r = 0.97$, $RMSD = 31.46$ mm, and $\sigma = 88.77$ mm (reference to GPCC $\sigma = 63.97$ mm) for CMIP5 and $r = 0.98$, $RMSD = 30.42$ mm, and $\sigma = 89.97$ mm for CMIP6. Similarly, the advancement from CMIP5 to CMIP6 in Zone II was indicated by the following results: $r = 0.96$–0.98, $RMSD = 36.41$–30.74 mm, and $\sigma = 104.49$–114.31 mm (σ of GPCC $= 118.55$ mm). Among the three zones, Zone I had poor accuracy with $r = 0.95$ and 0.97, $RMSD = 38.42$ mm and 41.69 mm, and $\sigma = 115.82$ mm and 131.29 mm (σ of GPCC $= 109.90$ mm) for CMIP5 and CMIP6, respectively. In summary, there was an improvement in the performance of the new CMIP6 over the previous CMIP5 for precipitation simulations over the MRB. CMIP6 thus better represented precipitation in the middle and downstream areas compared to CMIP5.

3.3. Performance of discharge simulation

Daily precipitation from all GCMs was used as input to the calibrated and validated RRI model to assess river flow and annual peak flood discharge. Fig. 6 shows a comparison of the gauged observation and simulated discharge at Kratie on monthly basis. During the flood season, the CMIP5 underestimated the river discharge by means and even error bars (i.e., mean ± standard deviation) in July and August, with values outside the range compared to the observation discharge. However, the mean values are overestimated in September but within the error bar, but closer to observations in the late flood period in October. The overall performance of CMIP6 improved during the flood season compared to that of CMIP5 – all values within the error bar. Notably, during the peak flood period in September, the mean of CMIP6 was close to the observation, whereas the mean of CMIP5 was underestimated.

Similar to precipitation and monthly discharge, the annual peak discharge (Fig. 7) showed a similar performance improvement in CMIP6 compared to CMIP5 at hydrological stations in Kratie and Chiang Saen. The simulated annual peak discharge from CMIP5 and CMIP6 overestimated the annual peak discharge at Chiang Saen. The mean values slightly improved from CMIP5 (14,398 m^3/s) to CMIP6 (13,890 m^3/s) compared to observation (10,483 m^3/s). At Kratie, the CMIP5 outputs underestimated the annual peak discharge, and the means from CMIP6 were in good agreement with the observations. The means from CMIP5 and CMIP6 were 37,220 m^3/s and 43,016 m^3/s compared to the observation of 43,521 m^3/s. However, the standard deviation values (ranging from lower to upper error bars) of the CMIP6 outputs at Kratie were larger than those of CMIP5 and of the observed peak discharges. Overall, even though there was an improvement in CMIP6 over CMIP5, CMIP6 still had an extensive bias compared to the observation. Therefore, the following sections consider the bias correction to further improve CMIP6 for the evaluation of future flooding projections in the MRB.

3.4. Performance of bias correction

The bias correction of the precipitation of CMIP6 was conducted using the linear scaling method to improve the performance of the precipitation and discharge projections. This method previously exhibited good performance in the bias correction of high-resolution climate outputs in the MRB (Try et al., 2020b). Fig. 8 shows the performance of simulated discharge from the non-bias corrected and

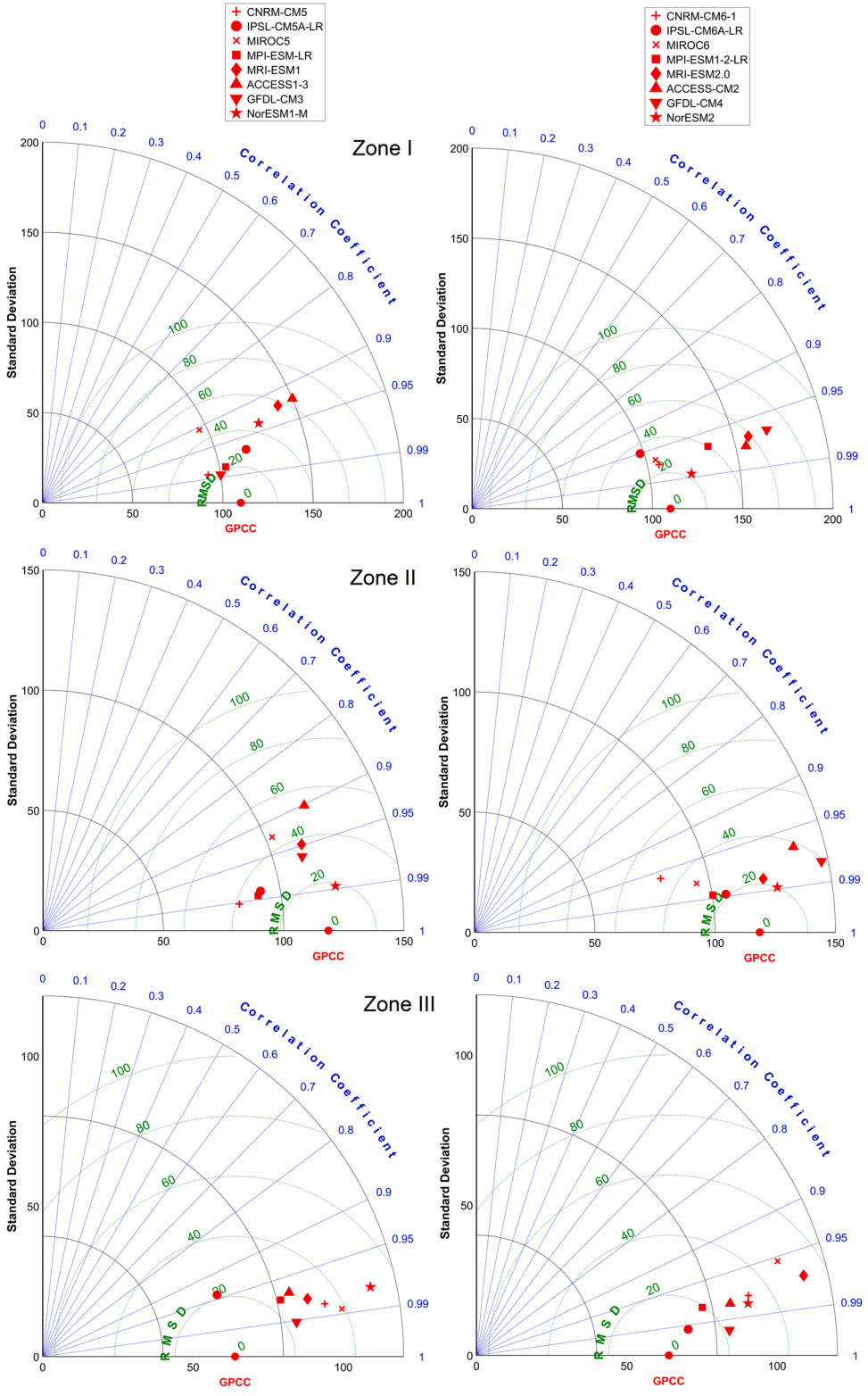

Fig. 5. Taylor diagram of average monthly precipitation for each zone (I, II, and III) for CMIP5 (left column) and CMIP6 (right column).

Table 3
Comparison of monthly precipitation from CMIP5 and CMIP6 based on each zone: Zone I (upper basin), Zone II (middle basin), and Zone III (lower basin) of the MRB.

GCMs		*r* [-]	*RMSD* [mm]	σ [mm]		*r* [-]	*RMSD* [mm]	σ [mm]
Zone I	GPCC	–	–	109.90		–	–	109.90
	CMIP5	0.99	23.85	93.07	CMIP6	0.97	25.22	106.37
		0.97	29.76	116.60		0.95	34.87	97.93
		0.91	46.44	95.79		0.97	28.28	105.05
		0.98	21.57	103.48		0.97	40.29	135.15
		0.92	57.71	141.12		0.97	58.90	158.20
		0.92	63.57	148.83		0.97	54.38	155.66
		0.99	19.19	99.99		0.97	68.93	168.94
		0.94	45.27	127.65		0.99	22.62	123.06
	avg.	0.95	38.42	115.82		0.97	41.69	131.29
Zone II	GPCC	–	–	118.55		–	–	118.55
	CMIP5	0.99	38.59	82.32	CMIP6	0.96	46.88	80.50
		0.98	32.63	91.83		0.99	21.23	105.65
		0.93	45.44	102.82		0.98	33.20	94.50
		0.99	32.60	90.51		0.99	24.91	100.25
		0.95	37.54	113.28		0.98	22.33	122.02
		0.90	53.02	120.34		0.97	38.17	137.18
		0.96	32.69	111.96		0.98	39.10	147.16
		0.99	18.76	122.88		0.99	20.10	127.21
	avg.	0.96	36.41	104.49		0.98	30.74	114.31
Zone III	GPCC	–	–	63.97		–	–	63.97
	CMIP5	0.98	34.58	95.40	CMIP6	0.98	33.09	92.58
		0.94	21.39	61.50		0.99	10.80	70.93
		0.99	38.87	100.70		0.95	47.87	104.92
		0.97	24.14	81.27		0.98	19.42	76.75
		0.98	30.80	90.11		0.97	52.11	112.00
		0.97	27.82	84.60		0.98	26.73	86.13
		0.99	23.44	85.19		1.00	21.84	84.55
		0.98	50.60	111.39		0.98	31.51	91.94
	avg.	0.97	31.46	88.77		0.98	30.42	89.97

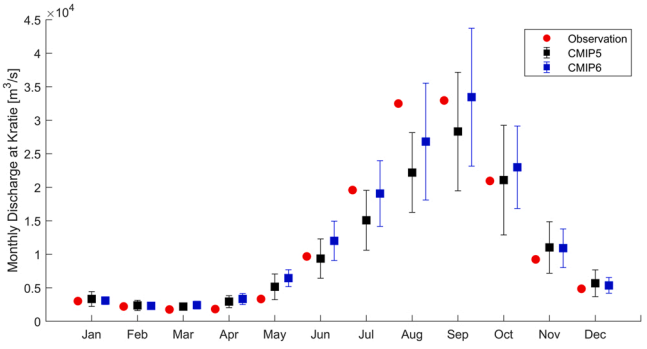

Fig. 6. Comparison of observed and simulated monthly discharge at Kratie from CMIP5 and CMIP6. The central point represents a mean, and its lower and upper bars display a mean ± standard deviations from model ensembles.

bias-corrected CMIP6. The non-bias corrected GCMs generally had more variation between each GCM in discharge simulation for both CMIP5 and CMIP6. In contrast, the bias corrected GCMs had smaller variations and were close to the ones generated from the GPCC dataset.

3.5. Projection of future precipitation

To better represent the precipitation effect on flooding, this study evaluated the changes in precipitation based on annual maximum 90-day rainfall, which provided the highest correlation with annual peak discharge and inundation compared with the periods from 1 to 6 months (Try et al., 2020c). Fig. 9 shows the annual maximum 90-day precipitation from the baseline period (1980–2014) to the projected periods in the near future (2026–2050), mid-future (2051–2075), and far future (2076–2100), derived from CMIP6. Overall, the results indicated that precipitation would increase for all future projected periods in the SSP2-4.5 and SSP5-8.5 scenarios. According to eight simulations from CMIP6, the effective precipitation would increase by 5%, 8%, and 9% for SSP2-4.5, and 6%, 9%, and 15% for SSP5-8.5 in near, mid, and far future, respectively. The results of the K–S test of annual maximum 90-day precipitation from

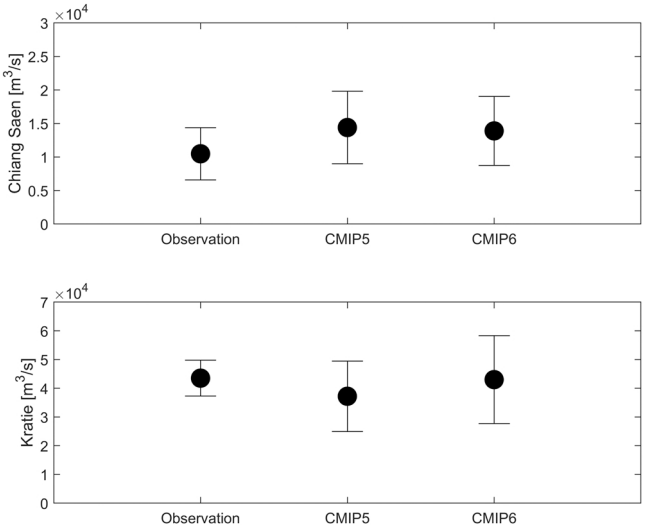

Fig. 7. Comparison of annual peak discharge at Chiang Saen and Kratie between observation and simulation from CMIP5 and CMIP6. The central point represents the mean, and its lower and upper bars display the mean ± standard deviations.

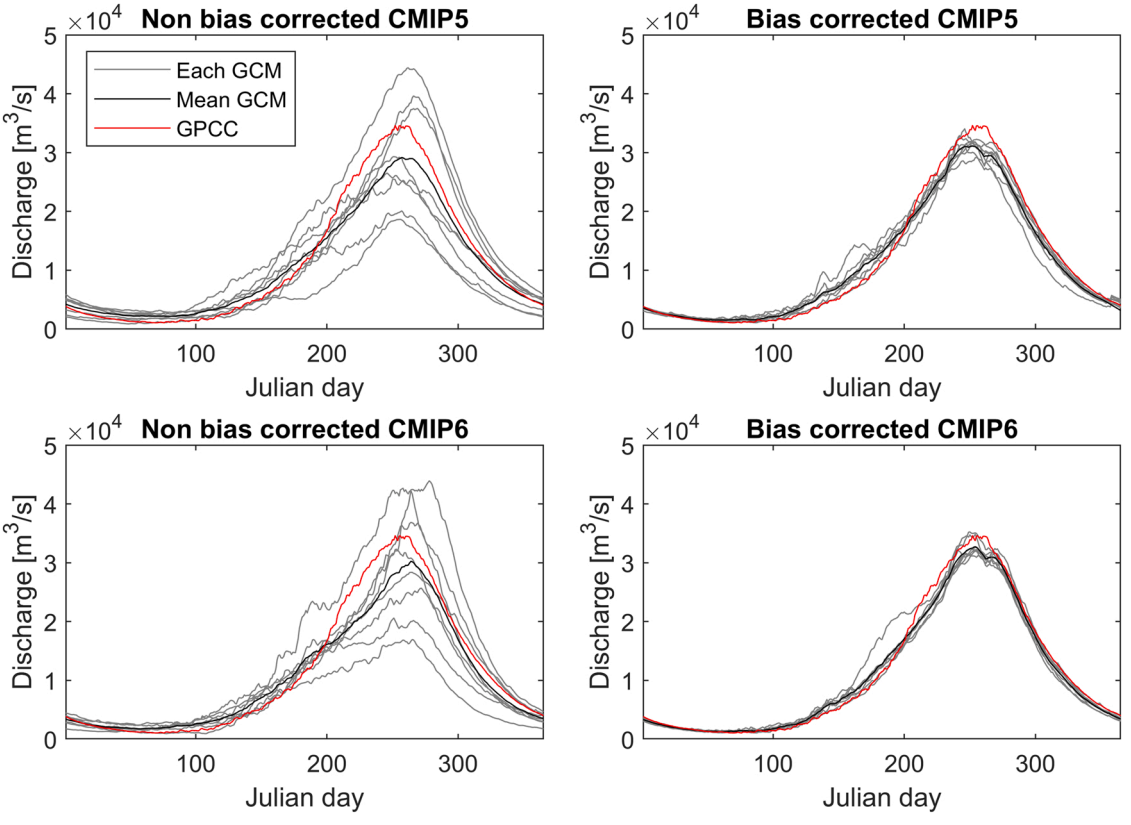

Fig. 8. Comparison of daily discharge at Kratie for non bias corrected and bias corrected GCMs from CMIP5 and CMIP6.

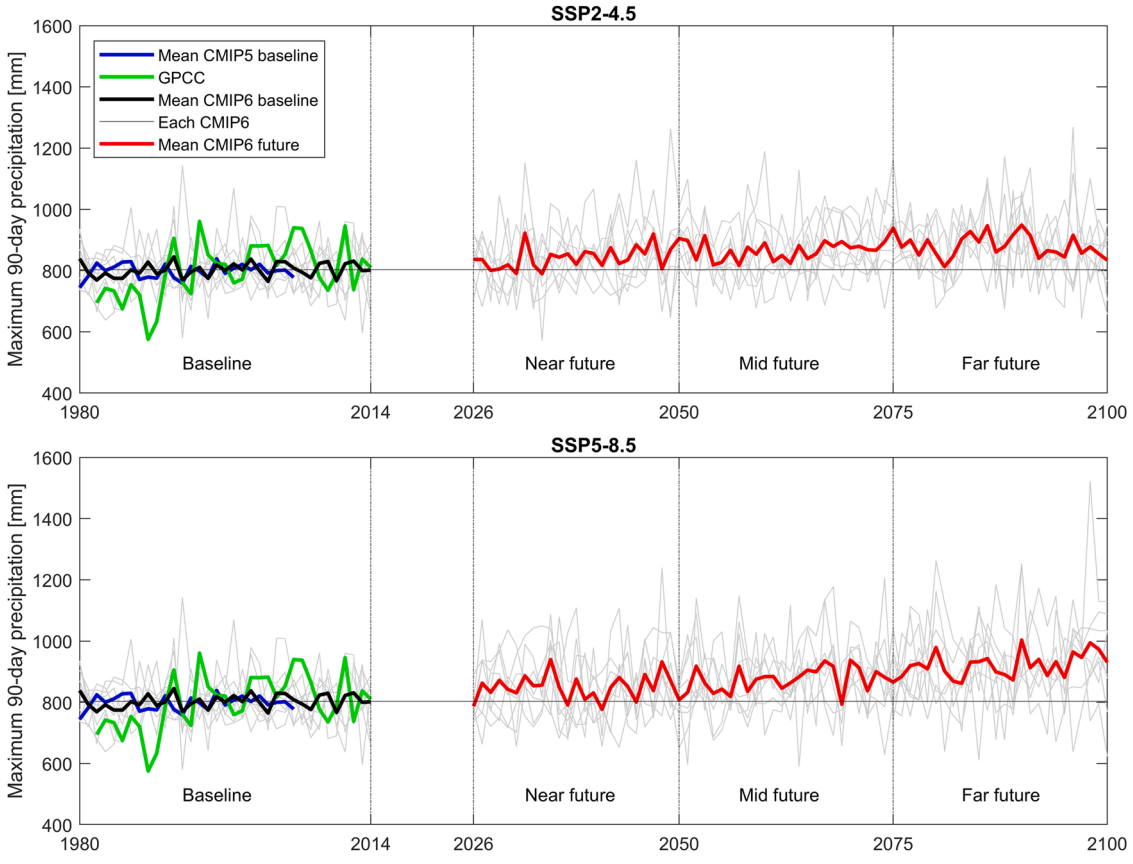

Fig. 9. Annual maximum 90-day precipitation from baseline to projections in the near, mid, and far future for SSP2-4.5 and SSP5-8.5. The horizontal straight lines represent means in the baseline period. The bold central lines are the means of model ensembles.

Table 4
Comparison of future projection of flood components in the near, mid, and far future projections.

Flood components		Near future	Mid future	Far future
Maximum 90-day precipitation	SSP2-4.5	+ 5%**	+ 8%**	+ 9%**
	SSP5-8.5	+ 6%**	+ 9%**	+ 15%**
Peak discharge at Chiang Saen	SSP2-4.5	+ 10%*	+ 20%**	+ 27%**
	SSP5-8.5	+ 10%**	+ 27%**	+ 47%**
Peak discharge at Vientiane	SSP2-4.5	+ 11%*	+ 22%**	+ 29%**
	SSP5-8.5	+ 14%*	+ 29%**	+ 54%**
Peak discharge at Pakse	SSP2-4.5	+ 15%**	+ 22%**	+ 26%**
	SSP5-8.5	+ 20%**	+ 27%**	+ 46%**
Peak discharge at Kratie	SSP2-4.5	+ 14%**	+ 21%**	+ 24%**
	SSP5-8.5	+ 18%**	+ 24%**	+ 41%**

Note: the values in the table represent the change in precipitation and peak discharge for each future projected period compared with baseline period. The asterisks * and ** represent p-value < 0.01 and < 0.001 of statistical K-S test.

the present to each future climate showed that the null hypothesis was rejected at a significance level of 1% for all cases of SSP2-4.5 and SSP5-8.5 during the near, mid, and far future (p-value < 0.001 in Table 4).

3.6. Projection of future floods

The peak discharge for future flood projections was evaluated and compared with the baseline period. Four main hydrological stations along the mainstream of the Mekong River were investigated. The annual peak discharge at Chiang Saen showed an increase in discharge by 10%, 20%, and 27% for SSP2-4.5, and 10%, 27%, and 47% for SSP5-8.5 at the projected periods in the near, mid, and far future, respectively (Fig. 10). These increases were notable with the K–S test at a significance level of 1%, with p-values < 0.01 (Table 4). Moreover, the peak discharge indicated a crucial increase in future projections with a similar rising rate of 11 – 29% for

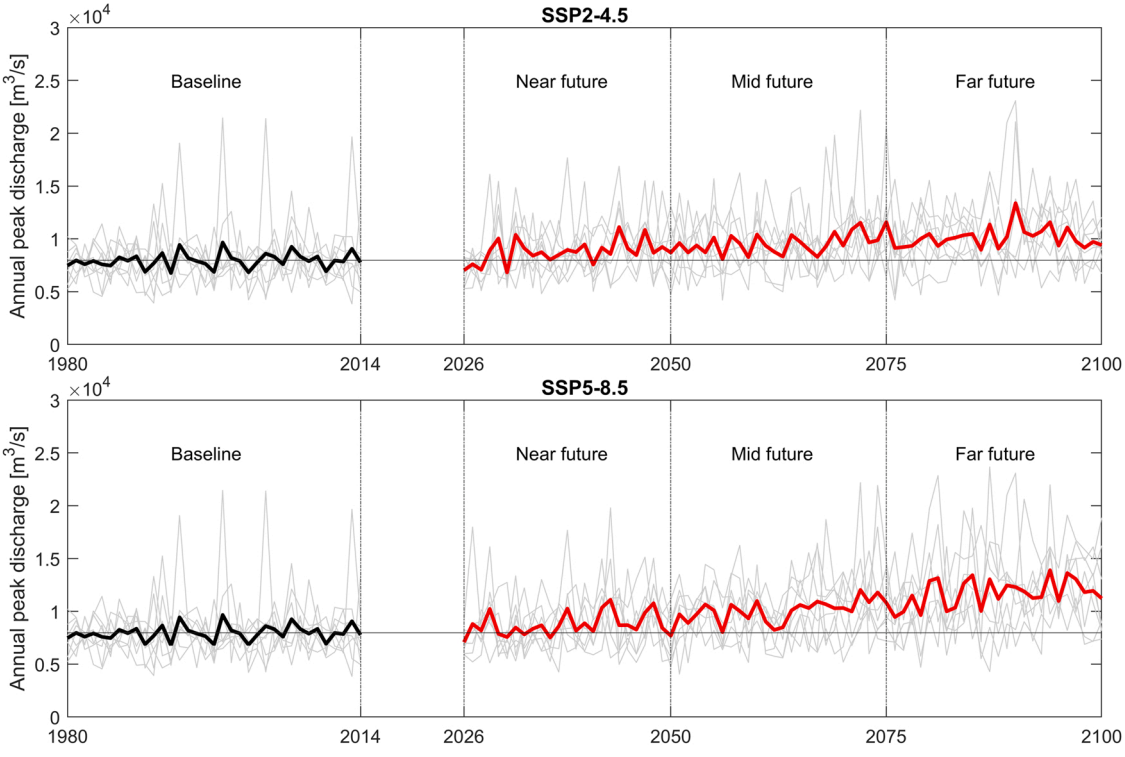

Fig. 10. Annual peak discharge at Chiang Saen from baseline to projections in the near, mid, and far future for SSP2-4.5 and SSP5-8.5. The horizontal straight lines represent the means in the baseline period. The bold central lines are the means of model ensembles.

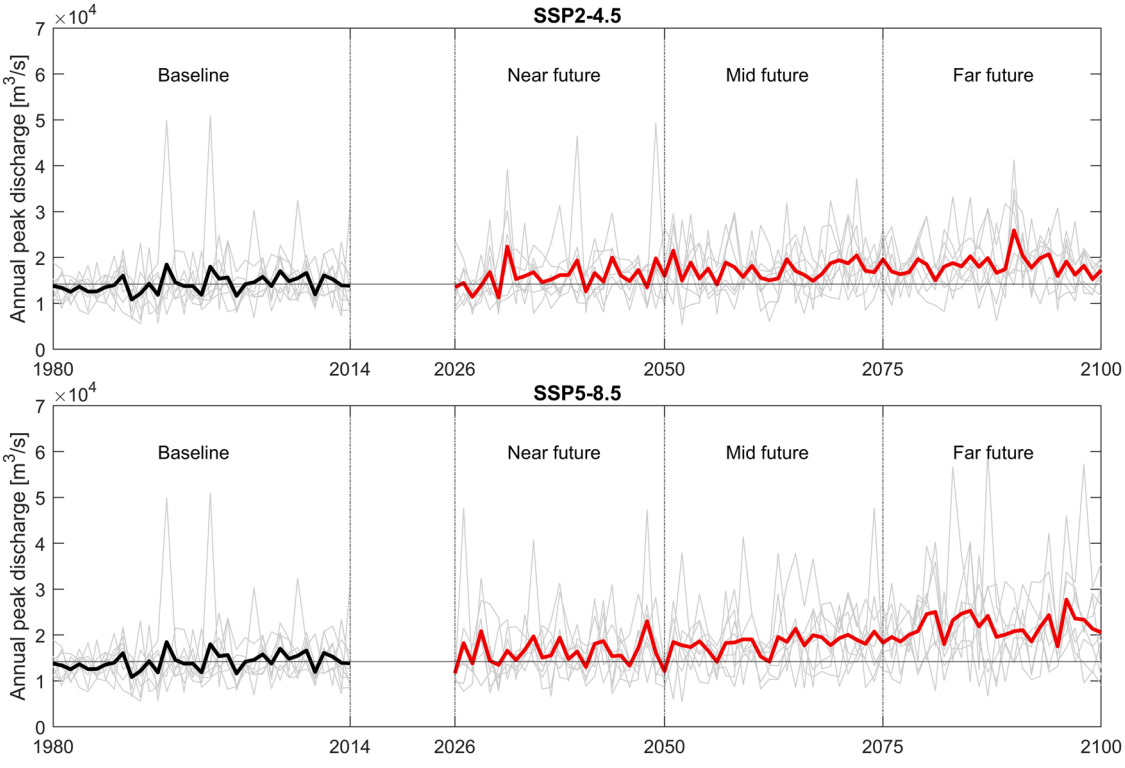

Fig. 11. Annual peak discharge at Vientiane from baseline to projections in the near, mid, and far future for SSP2-4.5 and SSP5-8.5. The horizontal straight lines represent the means in the baseline period. The bold central lines are the means of model ensembles.

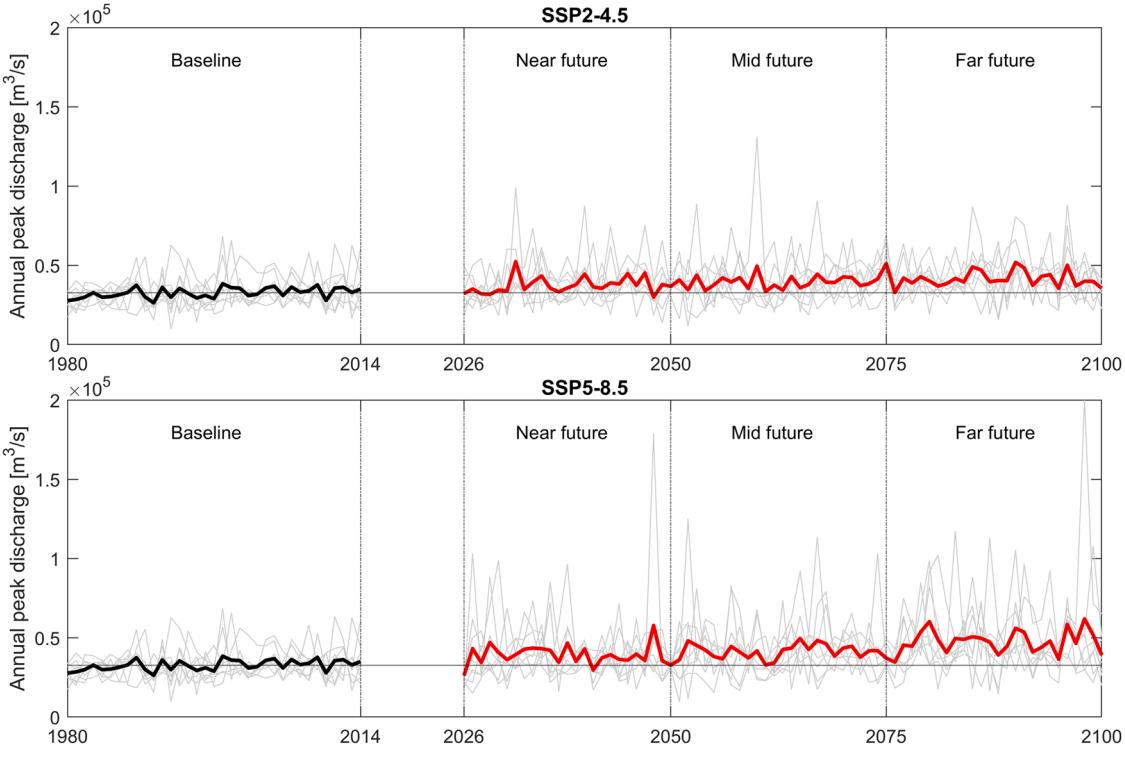

Fig. 12. Annual peak discharge at Pakse from baseline to projections in the near, mid, and far future for SSP2-4.5 and SSP5-8.5. The horizontal straight lines represent the means in the baseline period. The bold central lines are the means of model ensembles.

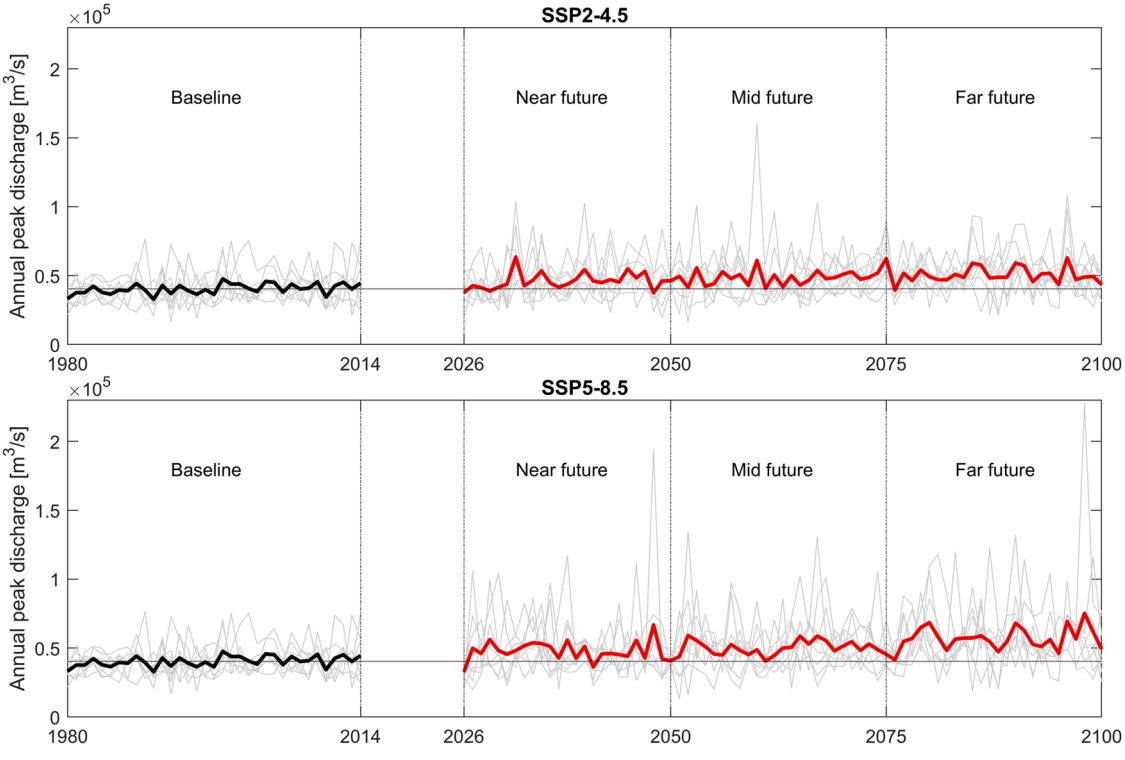

Fig. 13. Annual peak discharge at Kratie from baseline to projections in the near, mid, and far future for SSP2-4.5 and SSP5-8.5. The horizontal straight lines represent the means in the baseline period. The bold central lines are the means of model ensembles.

SSP2-4.5 and 14 − 54% for SSP5-8.5 in Vientiane (Fig. 11) (p-value < 0.01), 15 − 26% for SSP2-4.5, and 20 − 46% for SSP5-8.5 in Pakse (Fig. 12) (p-value < 0.001 in Table 4).

The peak discharge increased for all assessed periods at all stations (Figs. 10–13). In Fig. 13, the annual peak discharge in the downstream station Kratie is used as a representative point of flooding in the LMB. For the SSP2-4.5 scenario, the peak discharge increased by 14%, 21%, and 24% in the near, mid, and far future, respectively (p-value < 0.001). Additionally, the peak discharge for SSP5-8.5 sharply increased by 18%, 24%, and 41% for the three future projection periods (p-value < 0.001).

4. Discussion

4.1. Implementation of climate change impacts on future flood projections

The most recent CMIP6 have improved the characteristics and performance of climate simulations over the previous CMIP5. This study compared precipitation and flood characteristics from eight CMIP6 with the same models from CMIP5 in the MRB. According to the precipitation analysis based on the grid by grid, basin average, and three MRB zones, the CMIP6 results clearly show significant improvement in correlation and bias values. Moreover, the monthly and annual peak discharges from historical experiments have also improved; this was primarily observed in the model ensemble means from CMIP5, which underestimated peak flows compared to CMIP6.

The climate outputs of CMIP6 have significantly improved results compared to those of CMIP5, as confirmed by other research studies. Chen et al. (2021) showed similar improvements in extreme seasonal precipitation in CMIP6 over CMIP5 based on case studies in the Western North Pacific and East Asia. Xin et al. (2020) evaluated and found higher skill scores in the simulation of summer precipitation from CMIP6 in China and East Asia. Zamani et al. (2020) determined the outperformance of CMIP5 by CMIP6 for precipitation projections in northeastern Iran. Ayugi et al. (2021) showed an improved performance using CMIP6 in simulating mean and

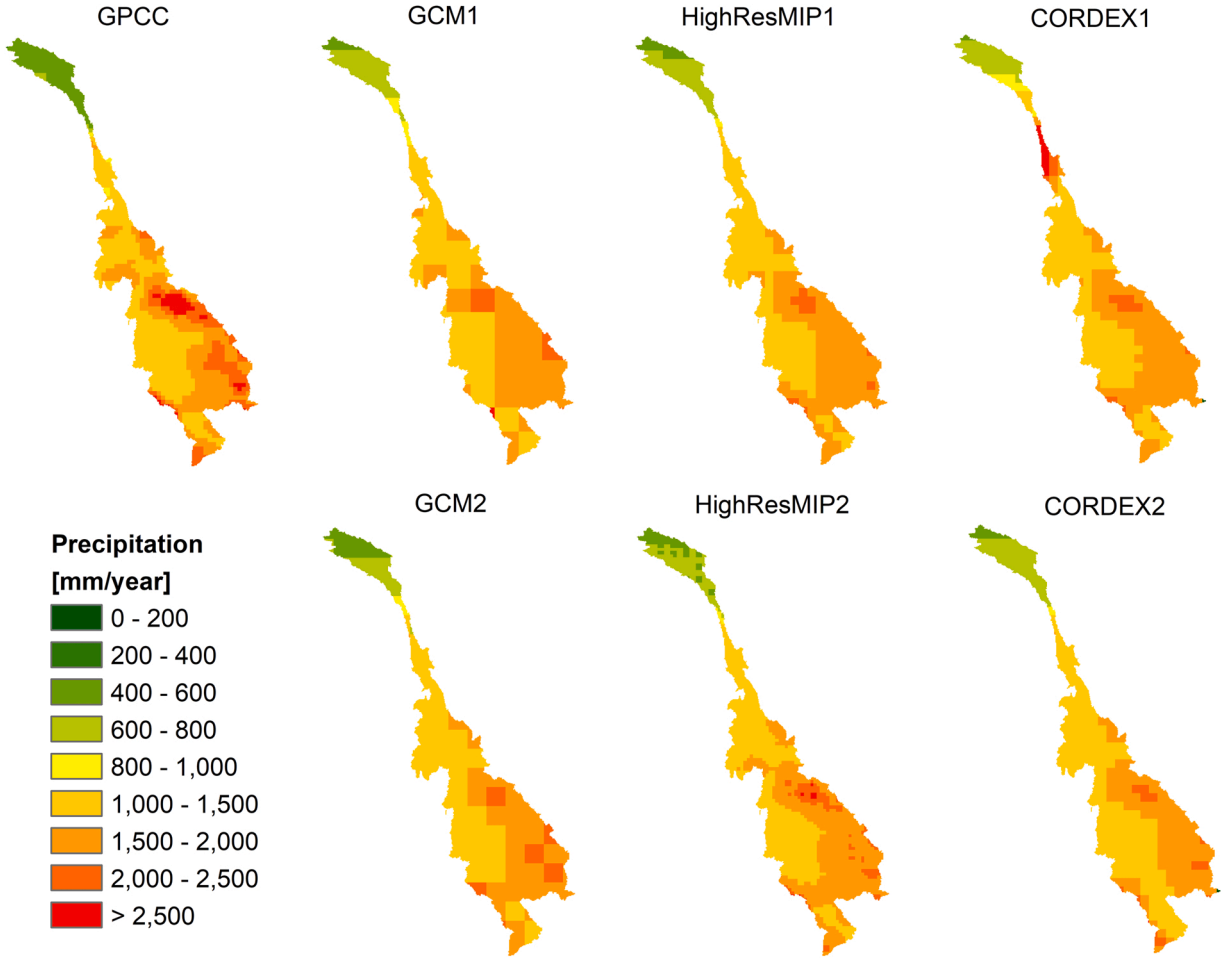

Fig. 14. Spatial distribution of annual precipitation from two coarse resolution GCMs (GCM1 and GCM2), two high resolution GCMs (HighResMIP1 and HighResMIP2), and two CORDEX RCMs (CORDEX1 and CORDEX2) compared with GPCC data over the MRB.

extreme precipitation in East Africa, with less bias than CMIP5.

Future climate projections in the MRB using the CMIP6 indicate an increase in both effective precipitation and annual peak discharge in the near (2026–2050), mid (2051–2075), and far (2076–2100) future compared to the baseline period (1980–2014). The increases in peak discharge at Kratie range between 14% and 24% and 18–41% during the three projected periods for SSP2-4.5 and SSP5-8.5, respectively. These results agree with those of previous studies on the impacts and severity of future climate change in the MRB. For instance, Try et al. (2020b) found an increase in high flow exceeding 5% of times (Q_5) by 13–30% in the future climate projection for 2075–2099 compared to 1979–2003. Similarly, Perera et al. (2017) found an increase in future inundation extent in the LMB between 24% and 35% by using a single MRI-AGCM3.2S with ranging of different sea surface temperature patterns with for RCP8.5, which is comparable to SSP5-8.5 in CMIP6. Västilä et al. (2010) projected annual maximum floods in the LMB from 2010 to 2049 with exceedance between 3% and 14% for the A2 scenario in CMIP3 (comparable to RCP8.5 in CMIP5 and SSP5-8.5 in CMIP6). Khoi et al. (2020) found an increase of annual river discharge of the MRB from 3.35% to 9.13% under RCP4.5 and RCP8.5 using CORDEX datasets.

4.2. Performance of CMIP6 GCMs and high resolution GCMs and RCMs

This study evaluated the effect of spatial resolution on flood simulation by comparing two high resolution version HighResMIP from CMIP6 (CNRM-CM6-1-HR and MRI-AGCM3.2S, hereafter noted as HighResMIP1 and HighResMIP2) and two RCMs from CORDEX East Asia (CNRM-CERFACS-CNRM-CM5 and MPI-M-MPI-ESM-LR, hereafter noted as CORDEX1 and CORDEX2) with the coarse resolution CMIP6 (CNRM-CM6-1 and MRI-ESM2-0, hereafter noted as GCM1 and GCM2). This analysis applied the same linear scaling bias correction method for the CMIP6, HighResMIP, and CORDEX. By comparing with GPCC precipitation, the HighResMIP and CORDEX datasets with high resolution of up to 0.1875–0.5° could overcome the smoothing distribution of annual precipitation, compared to the coarse resolution versions of CMIP6 (1.40625° and 1.125°) during the baseline period (Fig. 14). However, the difference in resolution was not sensitive to the basin average monthly precipitation. Even though the spatial resolution is different, the GCMs from the same model agency (i.e., GCM1 vs HighResMIP1 and GCM2 vs HighResMIP2) generally showed a similar precipitation distribution; no significant difference could be seen in the violin and box plots in Fig. 15. The mean monthly precipitation was 122 and 123 mm/month for HighResMIP1 and HighResMIP2, 122 and 123 mm/month for GCM1 and GCM2, and 126 and 119 mm/month for CORDEX1 and CORDEX2, respectively, compared to 126 mm/month from GPCC precipitation (Fig. 15). In addition, the discharge simulation performances from GCM, HighResMIP, and CORDEX showed a similar pattern of distribution, as shown in the violin plot of daily discharge in Fig. 16. Comparing with mean daily discharge from GPCC of 11,512 m^3/s, the simulated discharge was 11,773 and 11,487 m^3/s for GCM1 and GCM2, and 11,327 and 10,918 m^3/s for HighResMIP1 and HighResMIP2, and 13,509 and 10,577 m^3/s for CORDEX1 and CORDEX2, respectively (Fig. 16). In conclusion, the effect of different resolutions from GCMs and RCMs may not be a significant factor affecting flood projection in the MRB, particularly at Kratie station located near the floodplain of the LMB.

4.3. Uncertainties and limitations

This study primarily evaluated historical simulation from climate datasets and future projections of GCMs under future climate change impacts. Only future climate change impact perspectives on flooding were considered while leaving important variables untouched. The sources of uncertainties in flood projections under the impacts of climate change could be associated with emission scenarios, GCMs, downscaling methods, and hydrological models (Hoan et al., 2020). This study evaluated only two future projection scenarios (SSP2-4.5 and SSP5-8.5) from CMIP6. Other future projection scenarios (e.g., SSP1-2.6 and SSP3-7.0) could also possibly happen, and they should be considered in further studies. Moreover, different downscaling methods should be investigated to capture

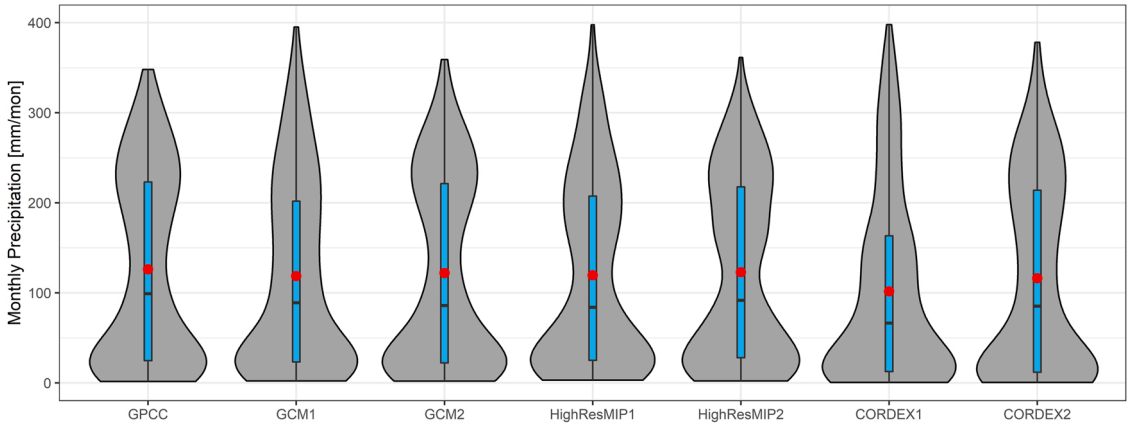

Fig. 15. Violin plot and boxplot of monthly from two coarse resolution GCMs (GCM1 and GCM2), two high resolution GCMs (HighResMIP1 and HighResMIP2), and two CORDEX RCMs (CORDEX1 and CORDEX2) compared with GPCC over the MRB. The red circle and black dots represent mean and median. The body side of violin displays the density distribution of data.

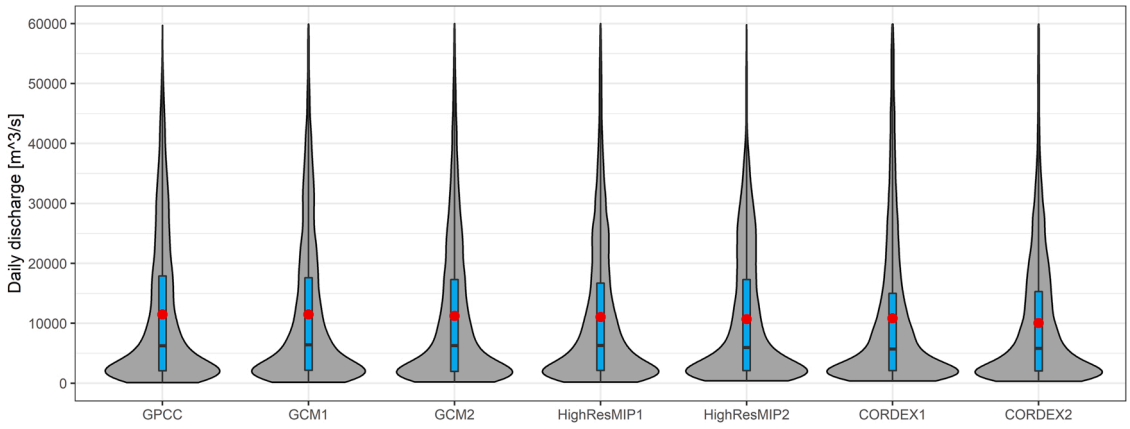

Fig. 16. Violin plot and boxplot of daily discharge at Kratie from two coarse resolution GCMs (GCM1 and GCM2), two high resolution GCMs (HighResMIP1 and HighResMIP2), and two CORDEX RCMs (CORDEX1 and CORDEX2) compared with GPCC. The red circle and black dots represent mean and median. The body side of violin displays the density distribution of data.

the topographic characteristics' complexity, particularly in the more regional-scale studies. Only the RRI model was used to project floods in this study, while different hydrological models and their input parameters could associate with flood projection uncertainties. In addition, land use was assumed to be constant from baseline throughout the projected periods in the RRI model simulation. Changes in topography due to soil erosion and deposition were not considered in the RRI model as well. Moreover, the influence of hydropower and irrigation reservoirs on the river basin's seasonal hydrology and flow has not yet been analyzed. The future projections of flooding in this study focused only on annual peak discharge using CMIP6. Further studies are needed to assess the cumulative impacts of climate change associated with these land-use changes and the impacts of water infrastructure development.

5. Conclusions

This study focuses on assessing the performance of eight CMIP6 compared with CMIP5 in precipitation and discharge simulations in the MRB. The results show a significant improvement in the non bias corrected CMIP6 compared to the non bias corrected CMIP5. The future projections of flooding in the MRB from eight CMIP6 show a significant increase in effective precipitation and annual peak discharge in the near, mid, and far future in both the SSP2-4.5 and SSP5-8.5 scenarios.

This study found that different resolutions of GCMs and RCMs performed similarly in predicting river discharge downstream of the MRB. However, our study focused on flood projection in the large basin (MRB) with a drainage area up to 795,000 km^2. The benefits of using high resolution GCM and regional downscaled climate data would be able to capture the complexity of land surface and local topographic characteristics in the small river basin, such as tributaries of the MRB.

Studies on climate change impacts on hydrology changes such as floods and droughts using CMIP6 could provide additional analysis to the previous CMIP3 or CMIP5 outputs. Moreover, further studies should focus on downscaling GCM to catch up with regional climate change by obtaining a higher spatial resolution; this might be more suitable for spatial distribution, particularly for studies in small-scale river basins. To reduce the possibility of severe damage caused by extreme flooding, adequate water resource management, flood adaptation and mitigation strategies, flood prevention infrastructure, and efficient real-time flood early warning and forecasting systems are required.

Funding

This research was supported by the Japan Society for the Promotion of Science (JSPS) KAKENHI Grant-in-Aid id: 21F21071. Sophal Try would like to thank to Japan International Cooperation Agency (JICA) under AUN/NEED-Net Program Phase 3 during Ph.D. scholarship program at Kyoto University.

Declaration of Competing Interest

The authors declare that they have no known competing financial interests or personal relationships that could have appeared to influence the work reported in this paper.

Acknowledgements

The authors would like to thank to two reviewers for their thoughtful and constructive comments and efforts towards improving this manuscript. The authors thank the Mekong River Commission for providing hydrological data. The climate datasets used in this study were freely downloadable at https://esgf-node.llnl.gov/search/cmip6/ for CMIP6, https://esgf-node.llnl.gov/search/cmip5/ for

CMIP5, and https://esg-dn1.nsc.liu.se/search/cordex/ for CORDEX.

Appendix A. Supporting information

Supplementary data associated with this article can be found in the online version at doi:10.1016/j.ejrh.2022.101035.

References

Ayugi, B., Zhidong, J., Zhu, H., Ngoma, H., Babaousmail, H., Rizwan, K., Dike, V., 2021. Comparison of CMIP6 and CMIP5 models in simulating mean and extreme precipitation over East Africa. Int. J. Climatol. 41, 6474–6496.
Bentsen, M., Bethke, I., Debernard, J.B., Iversen, T., Kirkevåg, A., Seland, Ø., Drange, H., Roelandt, C., Seierstad, I.A., Hoose, C., Kristjánsson, J.E., 2013. The Norwegian Earth System Model, NorESM1-M – Part 1: description and basic evaluation of the physical climate. Geosci. Model Dev. 6, 687–720.
Bi, D., Dix, M., Marsland, S.J., O'Farrell, S., Rashid, H., Uotila, P., Hirst, A.C., Kowalczyk, E., Golebiewski, M., Sullivan, A., 2013. The ACCESS coupled model: description, control climate and evaluation. Aust. Meteorol. Oceanogr. J. 63, 41–64.
Chadwick, M., Juntopas, M., 2008. Sustaining Tonle Sap: an assessment of development challenges facing the Great Lake. Sustain. Mekong Res. Netw. (Sumernet).
Chen, C.-A., Hsu, H.-H., Liang, H.-C., 2021. Evaluation and comparison of CMIP6 and CMIP5 model performance in simulating the seasonal extreme precipitation in the Western North Pacific and East Asia. Weather Clim. Extrem. 31, 100303.
Chen, H., Sun, J., Lin, W., Xu, H., 2020. Comparison of CMIP6 and CMIP5 models in simulating climate extremes. Sci. Bull. 65, 1415–1418.
Chhin, R., Oeurng, C., Yoden, S., 2020. Drought projection in the Indochina Region based on the optimal ensemble subset of CMIP5 models. Clim. Chang. 162, 687–705.
Chhin, R., Yoden, S., 2018. Ranking CMIP5 GCMs for model ensemble selection on regional scale: case study of the Indochina Region. J. Geophys. Res. Atmos. 123, 8949–8974.
Demory, M.-E., Berthou, S., Fernández, J., Sørland, S.L., Brogli, R., Roberts, M.J., Beyerle, U., Seddon, J., Haarsma, R., Schär, C., 2020. European daily precipitation according to EURO-CORDEX regional climate models (RCMs) and high-resolution global climate models (GCMs) from the High-Resolution Model Intercomparison Project (HighResMIP). Geosci. Model Dev. 13, 5485–5506.
Dong, T., Dong, W., 2021. Evaluation of extreme precipitation over Asia in CMIP6 models. Clim. Dyn. 1–19.
Donner, L.J., Wyman, B.L., Hemler, R.S., Horowitz, L.W., Ming, Y., Zhao, M., Golaz, J.-C., Ginoux, P., Lin, S.-J., Schwarzkopf, M.D., 2011. The dynamical core, physical parameterizations, and basic simulation characteristics of the atmospheric component AM3 of the GFDL global coupled model CM3. J. Clim. 24, 3484–3519.
Dufresne, J.-L., Foujols, M.-A., Denvil, S., Caubel, A., Marti, O., Aumont, O., Balkanski, Y., Bekki, S., Bellenger, H., Benshila, R., 2013. Climate change projections using the IPSL-CM5 Earth System Model: from CMIP3 to CMIP5. Clim. Dyn. 40, 2123–2165.
Dutta, D., Alam, J., Umeda, K., Hayashi, M., Hironaka, S., 2007. A two-dimensional hydrodynamic model for flood inundation simulation: a case study in the lower Mekong river basin. Hydrol. Process. Int. J. 21, 1223–1237.
Eyring, V., Bony, S., Meehl, G.A., Senior, C.A., Stevens, B., Stouffer, R.J., Taylor, K.E., 2016. Overview of the Coupled Model Intercomparison Project Phase 6 (CMIP6) experimental design and organization. Geosci. Model Dev. 9, 1937–1958.
Friedl, M.A., Sulla-Menashe, D., Tan, B., Schneider, A., Ramankutty, N., Sibley, A., Huang, X., 2010. MODIS Collection 5 global land cover: Algorithm refinements and characterization of new datasets. Remote Sens. Environ. 114, 168–182.
Giorgetta, M.A., Jungclaus, J., Reick, C.H., Legutke, S., Bader, J., Böttinger, M., Brovkin, V., Crueger, T., Esch, M., Fieg, K., 2013. Climate and carbon cycle changes from 1850 to 2100 in MPI-ESM simulations for the Coupled Model Intercomparison Project phase 5. J. Adv. Model. Earth Syst. 5, 572–597.
Giorgi, F., 2010. Uncertainties in climate change projections, from the global to the regional scale (Presented at the EPJ Web of conferences). EDP Sci. 115–129.
Gupta, H.V., Kling, H., Yilmaz, K.K., Martinez, G.F., 2009. Decomposition of the mean squared error and NSE performance criteria: implications for improving hydrological modelling. J. Hydrol. 377, 80–91.
Gusain, A., Ghosh, S., Karmakar, S., 2020. Added value of CMIP6 over CMIP5 models in simulating Indian summer monsoon rainfall. Atmos. Res. 232, 104680.
Haarsma, R.J., Roberts, M.J., Vidale, P.L., Senior, C.A., Bellucci, A., Bao, Q., Chang, P., Corti, S., Fučkar, N.S., Guemas, V., 2016. High resolution model intercomparison project (HighResMIP v1. 0) for CMIP6. Geosci. Model Dev. 9, 4185–4208.
Hoan, N.X., Khoi, D.N., Nhi, P.T.T., 2020. Uncertainty assessment of streamflow projection under the impact of climate change in the Lower Mekong Basin: a case study of the Srepok River Basin, Vietnam. Water Environ. J. 34, 131–142.
Hoang, L.P., Lauri, H., Kummu, M., Koponen, J., Van Vliet, M.T., Supit, I., Leemans, R., Kabat, P., Ludwig, F., 2016. Mekong River flow and hydrological extremes under climate change. Hydrol. Earth Syst. Sci. 20, 3027–3041.
IPCC, 2014. Synthesis Report. Contribution of Working Groups I, II and III to the Fifth Assessment Report of the Intergovernmental Panel on Climate Change. IPCC, Geneva, Switzerland.
Iqbal, Z., Shahid, S., Ahmed, K., Ismail, T., Ziarh, G.F., Chung, E.-S., Wang, X., 2021. Evaluation of CMIP6 GCM rainfall in mainland Southeast Asia. Atmos. Res. 254, 105525.
Johnstone, G., Puskur, R., Declerck, F., Mam, K., Mak, S., Pech, B., Seak, S., Chan, S., Hak, S., 2013. Tonle Sap Scoping Report-CGIAR Research Program on Aquatic Agricultural Systems. Consultative Group for International Agricultural Research, Montpellier, France.
Kamruzzaman, M., Shahid, S., Islam, A.T., Hwang, S., Cho, J., Zaman, Md.A.U., Ahmed, M., Rahman, Md.M., Hossain, Md.B., 2021. Comparison of CMIP6 and CMIP5 model performance in simulating historical precipitation and temperature in Bangladesh: a preliminary study. Theor. Appl. Climatol. 145, 1385–1406.
Keskinen, M., Kummu, M., Salmivaara, A., Someth, P., Lauri, H., de Moel, H., Ward, P., Sokhem, P., 2013. Tonle Sap now and in the future? Final Report of the Exploring Tonle Sap Futures study. Final Report of the Exploring Tonle Sap Futures Study, Aalto University and 100Gen Ltd. with Hatfield Consultants Partnership, VU University Amsterdam, EIA Ltd. and Institute of Technology of Cambodia, in partnership with Tonle Sap Authority and Supreme National Economic Council. Water & Development Publications WD-11, Aalto University, Espoo, Finland.
Khoi, D.N., Nguyen, V.T., Sam, T.T., Ky Phung, N., Thi Bay, N., 2020. Responses of river discharge and sediment load to climate change in the transboundary Mekong River Basin. Water Environ. J. 34, 367–380.
Kim, Y.-H., Min, S.-K., Zhang, X., Sillmann, J., Sandstad, M., 2020. Evaluation of the CMIP6 multi-model ensemble for climate extreme indices. Weather Clim. Extrem. 29, 100269.
Kobayashi, S., Ota, Y., Harada, Y., Ebita, A., Moriya, M., Onoda, H., Onogi, K., Kamahori, H., Kobayashi, C., Endo, H., 2015. The JRA-55 reanalysis: General specifications and basic characteristics. J. Meteorological Soc. Jpn. Ser. II 93, 5–48.
Liang, J., Tan, M.L., Hawcroft, M., Catto, J.L., Hodges, K.I., Haywood, J.M., 2021. Monsoonal precipitation over Peninsular Malaysia in the CMIP6 HighResMIP experiments: the role of model resolution. Clim. Dyn. 1–23.
Mizuta, R., Arakawa, O., Ose, T., Kusunoki, S., Endo, H., Kitoh, A., 2014. Classification of CMIP5 future climate responses by the tropical sea surface temperature changes. Sola 10, 167–171.
Mizuta, R., Yoshimura, H., Murakami, H., Matsueda, M., Endo, H., Ose, T., Kamiguchi, K., Hosaka, M., Sugi, M., Yukimoto, S., 2012. Climate simulations using MRI-AGCM3. 2 with 20-km grid. J. Meteorol. Soc. Jpn. Ser. II 90, 233–258.
MRC, 2010. State of the Basin Report 2010. Mekong River Commission, Vientiane, Lao PDR.

MRC, 2011. Planning atlas of the lower Mekong river basin. Mekong River Commission, Vientiane, Lao PDR.
Nash, J.E., Sutcliffe, J.V., 1970. River flow forecasting through conceptual models part I — a discussion of principles. J. Hydrol. 10, 282–290.
Oddo, P.C., Ahamed, A., Bolten, J.D., 2018. Socioeconomic impact evaluation for near real-time flood detection in the lower mekong river basin. Hydrology 5, 23.
O'Neill, B.C., Tebaldi, C., Vuuren, D.P., van, Eyring, V., Friedlingstein, P., Hurtt, G., Knutti, R., Kriegler, E., Lamarque, J.-F., Lowe, J., 2016. The scenario model intercomparison project (ScenarioMIP) for CMIP6. Geosci. Model Dev. 9, 3461–3482.
Perera, E.D.P., Sayama, T., Magome, J., Hasegawa, A., Iwami, Y., 2017. RCP8.5-based future flood hazard analysis for the lower Mekong River Basin. Hydrology 4, 55.
Pokhrel, Y., Shin, S., Lin, Z., Yamazaki, D., Qi, J., 2018. Potential disruption of flood dynamics in the lower Mekong River Basin due to upstream flow regulation. Sci. Rep. 8, 17767.
Ruan, Y., Yao, Z., Wang, R., Liu, Z., 2018. Ranking of CMIP5 GCM skills in simulating observed precipitation over the Lower Mekong Basin, using an improved score-based method. Water 10, 1868.
Sayama, T., Ozawa, G., Kawakami, T., Nabesaka, S., Fukami, K., 2012. Rainfall–runoff–inundation analysis of the 2010 Pakistan flood in the Kabul River basin. Hydrol. Sci. J. 57, 298–312.
Sayama, T., Tatebe, Y., Iwami, Y., Tanaka, S., 2015a. Hydrologic sensitivity of flood runoff and inundation: 2011 Thailand floods in the Chao Phraya River basin. Nat. Hazards Earth Syst. Sci. 15, 1617–1630.
Sayama, T., Tatebe, Y., Tanaka, S., 2015b. An emergency response-type rainfall-runoff-inundation simulation for 2011 Thailand floods. J. Flood Risk Manag. 10, 65–78.
Siev, S., Paringit, E.C., Yoshimura, C., Hul, S., 2019. Modelling inundation patterns and sediment dynamics in the extensive floodplain along the Tonle Sap River. River Res. Appl. 35, 1387–1401.
Tan, M.L., Liang, J., Samat, N., Chan, N.W., Haywood, J.M., Hodges, K., 2021. Hydrological extremes and responses to climate change in the Kelantan River Basin, Malaysia, based on the CMIP6 HighResMIP experiments. Water 13, 1472.
Tanaka, T., Yoshioka, H., Siev, S., Fujii, H., Fujihara, Y., Hoshikawa, K., Ly, S., Yoshimura, C., 2018. An integrated hydrological-hydraulic model for simulating surface water flows of a shallow lake surrounded by large floodplains. Water 10, 1213.
Taylor, K.E., 2001. Summarizing multiple aspects of model performance in a single diagram. J. Geophys. Res. Atmos. 106, 7183–7192.
Try, S., Daeup, Lee, Lee, G., 2018a. Application of nightlight satellite imagery for assessing flooding potential area in the Mekong river basin. J. Korea Water Resour. Assoc. 565–574.
Try, S., Lee, G., Yu, W., Oeurng, C., Jang, C., 2018b. Large-scale flood-inundation modeling in the Mekong River Basin. J. Hydrol. Eng. 23, 05018011.
Try, S., Tanaka, S., Tanaka, K., Sayama, T., Hu, M., Sok, T., Oeurng, C., 2020a. Projection of extreme flood inundation in the Mekong River basin under 4K increasing scenario using large ensemble climate data. Hydrol. Process. 34, 4350–4364.
Try, S., Tanaka, S., Tanaka, K., Sayama, T., Lee, G., Oeurng, C., 2020b. Assessing the effects of climate change on flood inundation in the lower Mekong Basin using high-resolution AGCM outputs. Prog. Earth Planet. Sci. 7, 34.
Try, S., Tanaka, S., Tanaka, K., Sayama, T., Oeurng, C., Uk, S., Takara, K., Hu, M., Han, D., 2020c. Comparison of gridded precipitation datasets for rainfall-runoff and inundation modeling in the Mekong River Basin. PLoS One 15, e0226814.
Uk, S., Yoshimura, C., Siev, S., Try, S., Yang, H., Oeurng, C., Li, S., Hul, S., 2018. Tonle Sap Lake: current status and important research directions for environmental management. Lakes Reserv. Res. Manag. 23, 177–189.
Västilä, K., Kummu, M., Sangmanee, C., Chinvanno, S., 2010. Modelling climate change impacts on the flood pulse in the Lower Mekong floodplains. J. Water Clim. Chang. 1, 67–86.
Voldoire, A., Sanchez-Gomez, E., Y Mélia, D.S., Decharme, B., Cassou, C., Sénési, S., Valcke, S., Beau, I., Alias, A., Chevallier, M., 2013. The CNRM-CM5. 1 global climate model: description and basic evaluation. Clim. Dyn. 40, 2091–2121.
Wang, D., Liu, J., Shao, W., Mei, C., Su, X., Wang, H., 2021a. Comparison of CMIP5 and CMIP6 multi-model ensemble for precipitation downscaling results and observational data: the case of Hanjiang River Basin. Atmosphere 12, 867.
Wang, J., Yun, X., Pokhrel, Y., Yamazaki, D., Zhao, Q., Chen, A., Tang, Q., 2021b. Modeling daily floods in the Lancang-Mekong River Basin using an improved hydrological-hydrodynamic model. Water Resour. Res. 57 e2021WR029734.
Watanabe, S., Hajima, T., Sudo, K., Nagashima, T., Takemura, T., Okajima, H., Nozawa, T., Kawase, H., Abe, M., Yokohata, T., 2011. MIROC-ESM 2010: model description and basic results of CMIP5-20c3m experiments. Geosci. Model Dev. 4, 845–872.
Xin, X., Wu, T., Jie, W., Zhang, J., 2021. Impact of higher resolution on precipitation over China in CMIP6 HighResMIP models. Atmosphere 12, 762.
Xin, X., Wu, T., Zhang, J., Yao, J., Fang, Y., 2020. Comparison of CMIP6 and CMIP5 simulations of precipitation in China and the East Asian summer monsoon. Int. J. Climatol. 40, 6423–6440.
Yamazaki, D., Ikeshima, D., Tawatari, R., Yamaguchi, T., O'Loughlin, F., Neal, J.C., Sampson, C.C., Kanae, S., Bates, P.D., 2017. A high-accuracy map of global terrain elevations. Geophysical Res. Letters 44, 5844–5853.
Yukimoto, S., Adachi, Y., Hosaka, M., Sakami, T., Yoshimura, H., Hirabara, M., Tanaka, T.Y., Shindo, E., Tsujino, H., Deushi, M., 2012. A new global climate model of the Meteorological Research Institute: MRI-CGCM3—model description and basic performance—. J. Meteorol. Soc. Jpn. Ser. II 90, 23–64.
Zamani, Y., Hashemi Monfared, S.A., Azhdari moghaddam, M., Hamidianpour, M., 2020. A comparison of CMIP6 and CMIP5 projections for precipitation to observational data: the case of Northeastern Iran. Theor. Appl. Climatol. 142, 1613–1623.
Ziese, M., Rauthe-Schöch, A., Becker, A., Finger, P., Meyer-Christoffer,A., Schneider, U., 2018. GPCC full data daily version. 2018 at 1.0∞: Daily land-surface precipitation from rain-gauges built on GTS-based and historic data. GPCC Full Data Daily Version. 2018 at 1.0°: Daily Land-Surface Precipitation from Rain-Gauges Built on GTS-Based and Historic Data.